Journal of Applied Electrochemistry **30**: 1053–1060, 2000.

A mathematical model for the internal cathodic protection of cylindrical structures by wire anodes

S. MARTINEZ* and I. ŠTERN
*Faculty of Chemical Engineering and Technology, Marulicev Trg 19, PO Box 177, HR-10000 Zagreb, Croatia (*author for correspondence, e-mail: smartin@pierre.fkit.hr)*

Received 2 June 1999; accepted in revised form 28 January 2000

Key words: cathodic protection, current distribution, modelling, potential distribution

Abstract

The applicability of a two-dimensional mathematical model of the impressed current cathodic protection (CP) system of the interior wall of a cylindrical structure was investigated. The modelled system was an axisymmetric cylindrical column filled with electrolyte with a wire anode running along its entire length and displaced from the column axis. Model inputs included anode and cathode dimensions, the anode-to-cathode distance, the electrolyte conductivity and limiting current density of oxygen reduction. A semi-analytical solution to the Laplace equation was used to compute the distribution of electrical potential. From these results, the nonuniform current density distribution was obtained to a first approximation by entering the computed values of the position-dependent cathode polarization potential into the nonlinear experimentally obtained polarization expression. The experimental electrical potential distribution compared well with that predicted by the model. Results showed the possibility of overprotection occurring in the system. The mathematical analysis was also extended to the case of a system with two wire anodes.

List of symbols

a	bipolar system parameter (cm)
A_0	first Fourier coefficient
A_m	mth Fourier coefficient
b_a	anodic Tafel slope (mV dec^{-1})
b_c	cathodic Tafel slope (mV dec^{-1})
d	anode-to-cathode distance (cm)
E	voltage (V)
E_a^e	equilibrium potential of the anodic reaction (mV)
E_c^e	equilibrium potential of the cathodic reaction (mV)
i	net current density (A cm^{-2})
$\boldsymbol{i}$	net current density vector (A cm^{-2})
$\boldsymbol{i}_a$	current density vector of iron dissolution (A cm^{-2})
$\boldsymbol{i}_c$	current density vector of hydrogen evolution (A cm^{-2})
i_{0a}	exchange current density of the anodic reaction (A cm^{-2})
i_{0c}	exchange current density of the cathodic reaction (A cm^{-2})
i_l	limiting current density of oxygen reduction (A cm^{-2})
$\boldsymbol{i}_l$	limiting current density vector of oxygen reduction (A cm^{-2})
i_0	constant value of current density (A cm^{-2})
m, n	integers
$\boldsymbol{n}$	outward normal to cathodic surface (cm)
r_a	anode radius (cm)
r_c	cathode radius (cm)
u	bipolar system coordinate
u_a	value of u at the anodic surface
u_c	value of u at the cathodic surface
v	bipolar system coordinate
x	cartesian system coordinate
y	cartesian system coordinate

Greek letters

$\Delta\Phi^{max}$	maximum difference of the cathodic polarization potentials (mV)
$\Delta\Phi_{red}^{max}$	reduced maximum difference of the cathodic polarization potentials (mV)
Φ	potential (mV)
Φ_a	potential at points adjacent to the anode (mV)
Φ_0	constant value of potential (mV)
κ	electrolyte conductivity (S cm^{-1})

1. Introduction

A starting point in considering the engineering of the internal cathodic protection (CP) of cylindrical structures is the centrally positioned wire anode. However, it is often difficult to support a wire anode in the centre of the structure (e.g., due to constructional or hydrodynamic reasons) and it may be more convenient to hold it somewhat off centre. For example, in water wells with casings, the anode is positioned between the casing and the wall of the pipe. Also, in horizontal pipes that are occasionally left partially filled with water it is useful to have the anode at the bottom of the pipe. In some cases it is considered prudent to place two anodes, usually adjacent to each other and equidistant from the axis of the structure, so that should one fail it is possible to operate backup protection from the other.

In big pipelines or tanks more than one anode is needed to meet the criterion of sufficient protection. Anodes can be positioned to have their cross-sections lie on a circumference of a radius $r < r_c$, centred at the cylinder axis. Two anodes are usually positioned to lie successively at 0° and 180°, three anodes at 0°, 120° and 240° etc.

In systems with one anode, as well as in systems with multiple anode arrangements, anodes should supply a uniform current density to the surface of the protected structure to maintain it within a specified potential range relative to the adjacent electrolytic medium. Designing CP systems [1] is based on calculation of the electrical potential and current distributions in the system, particularly on the surface of the protected structure.

The electrical potential and current distributions in an electrolytic cell with stagnant electrolyte [2] are determined by the current–potential curves of the cathode and the anode, conductivity of the electrolyte, and the geometry of the cell, while the ohmic potential drop in metallic parts of the system is usually disregarded.

At steady-state conditions, in an electrolyte with uniform concentration profile and constant specific conductivity, the governing equation for the distribution of the electrical potential Φ is the Laplace equation [3, 4]:

$$\nabla^2\Phi = 0 \tag{1}$$

subject to the boundary conditions prevailing on the cathode and anode surfaces.

In modelling of CP systems two simplified boundary conditions [2] are commonly used: (a) on the anodes, a constant potential, $\Phi = \Phi_0$ is taken, that is, such anodes are considered nonpolarizable, and (b) on the structure surface to be protected (cathode), a constant current density, $i = i_0$ is taken. For steel in neutral media the boundary condition (b) is often an adequate approximation when local limiting current densities corresponding to the local limiting rate of oxygen transport to the protected surface do not deviate too much from the average limiting current density i_l. The condition is applicable when nonnumerical methods are employed, and allows computation of the approximate nonuniform current distribution on the cathode by starting with a uniform distribution, calculating the corresponding potentials and introducing these values as a perturbation into the polarization expression $i = f(\Phi)$ for the cathode [2].

Most CP systems consist of complex geometrical arrangements of electrode surfaces with nonlinear boundary conditions, and their design requires the use of numerical methods, such as the finite difference method [5], the finite element method [6] and the boundary value method [7, 8]. However, for many practical cases, rather crude approximations introduced by nonnumerical methods are sufficient. A number of analytical and semi-analytical solutions to Equation 1 applied to CP systems are described in the works of Wagner [9, 10] and Newman [11, 12]. This work aims at investigating the possibility of utilization of one such solution in designing CP of the internal wall of a cylinder by wire anodes.

2. Mathematical development

To protect the surface of an internal wall of a cylinder, one or more anodes in the form of wires parallel to the cylinder axes and displaced from the center may be provided.

Figure 1 shows the cross-section of a cylinder of radius r_c which is to be protected cathodically by a parallel, cylindrical anode of radius r_a, displaced by distance d from the cylinder axis. If both electrodes extend from the surface of the electrolyte to the bottom of the cell, no dependence on the distance from the bottom is to be expected, so that the geometry may be

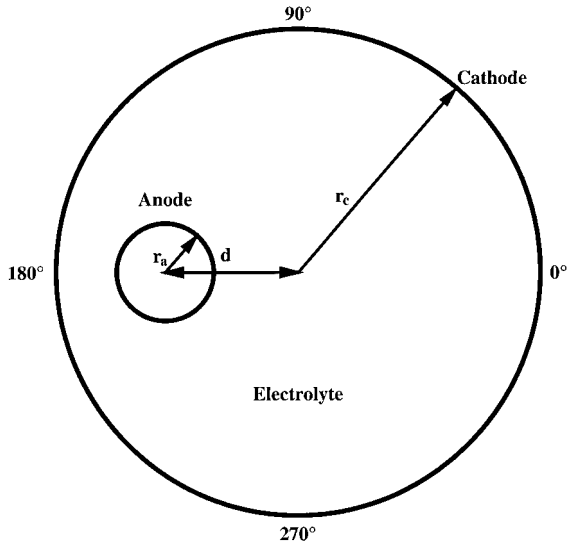

Fig. 1. Schematic view of a cross-section of the investigated CP system.

mapped onto a two-dimensional plane and the governing differential Equation 1 becomes:

$$\frac{\partial^2\Phi}{\partial x^2}+\frac{\partial^2\Phi}{\partial y^2}=0 \tag{2}$$

where x and y are the cartesian coordinates. At points in the electrolyte adjacent to the anode a constant potential, Φ_a, may be assumed yielding a boundary condition of the Dirichlet form [13]:

$$\Phi\big|_{\text{anode}}=\Phi_a \tag{3}$$

On the cathode, uniform current density is assumed yielding a boundary condition of the Neumann form [13]:

$$\left.\frac{\partial\Phi}{\partial \boldsymbol{n}}\right|_{\text{cathode}}=\frac{i_l}{\kappa} \tag{4}$$

where i_l is the current density required for cathodic protection on bare steel or on coated steel after taking into account the reduction in transport of oxygen to the surface of the cylinder introduced by the coating. κ is the electrolyte conductivity and $\boldsymbol{n}$ is the outward normal to the surface of the cathode. The solution is feasible in the coordinate system of bipolar circles [14, 15] and has been derived by Newman [11] for the case of a wire anode placed externally to the cylinder. In this work, a similar form of solution was adopted for the case of anodes placed internally. Laplace equation in the bipolar coordinate system [16] has the same form as the Equation 2, that is,

$$\frac{\partial^2\Phi}{\partial u^2}+\frac{\partial^2\Phi}{\partial v^2}=0 \tag{5}$$

where u and v are the bipolar coordinates related to cartesian coordinates by [15]

$$x=\frac{a\sinh(u)}{\cosh(u)-\cos(v)} \tag{6a}$$

$$y=\frac{a\sin(v)}{\cosh(u)-\cos(v)} \tag{6b}$$

These two relations are found by means of conformal mapping, so that the curves of $v=\text{const.}$ in the u–v plane are transformed into the circles passing through $x=a, y=0$ and $x=-a, y=0$ in the x–y plane. The curves of $u=\text{const.}$ in the u–v plane are transformed into the circles enclosing $x=a, y=0$ and the curves of $-u=\text{const.}$ are circles enclosing $x=-a, y=0$ in x–y plane [15]. The circle $u=u_c$ is the cathode itself and the circle $-u=u_a$ is the anode itself. Coordinate v determines the angular position of a point on a circle defined by the fixed value of u in the x–y plane. a is the parameter of the coordinate system which is determined by the geometric arrangement in Figure 1. The value of u_c is computed from the set of two coupled nonlinear equations:

$$\sinh(u_a)-\frac{r_c}{r_a}\sinh(u_c)=0 \tag{7a}$$

$$d-r_c\cosh(u_c)+r_a\cosh(u_a)=0 \tag{7b}$$

and the parameter a is then computed from the identity:

$$a=r_c\sinh(u_c) \tag{8}$$

The boundary condition on the anode remains the same as before (Equation 3), while that on the cathode (Equation 4) transforms into

$$\left.\frac{\partial\Phi}{\partial u}\right|_{u=u_c}=\frac{-i_l a/\kappa}{\cosh(u_c)-\cos(v)} \tag{9}$$

The solution to Equation 5 subject to the boundary conditions (3) and (9) is given in the form of a Fourier series:

$$\Phi=\Phi_a+A_0(u-u_a)+\sum_{m=1}^{\infty}A_m\sinh[m(u-u_a)]\cos(mv) \tag{10}$$

where A_m are Fourier coefficients. By subjecting Equation 10 to the boundary condition (9) and making use of the orthogonality of the cosine function, integral equations for coefficient A_m are obtained:

$$A_0=\frac{i_l a}{\kappa}\frac{1}{\pi}\int_0^{\pi}\frac{dv}{\cosh(u_c)-\cosh(v)} \tag{10a}$$

$$A_m=\frac{i_l a}{\kappa}\frac{2}{m\pi\cosh(u_c-u_a)}\int_0^{\pi}\frac{\cos(mv)}{\cosh(u_c)-\cosh(v)}dv \tag{10b}$$

The number of coefficients actually computed is determined by the desired calculation precision. All computations and graphical representations in this work were carried out using the programming system *Mathematica®*.

3. Experimental procedure

Two main types of measurements were conducted to verify the model. First, the current density–potential curves of the cylinder (pipe) material (low-carbon steel) and of high-purity iron were measured in order to determine the range of protection potentials. For this purpose, specimens were machined as 2 mm diameter cylinders. The cross-section of the cylinder was exposed to the solution while the rest of the electrode was sealed in epoxy resin. The electrode surface was polished with

abrasive paper and degreased in methanol. It was then placed into the solution, near the tip of a Luggin capillary that was mounted on a saturated calomel electrode. The electrolyte was NaCl in deionized water. The current density–potential curves were obtained by the application of a d.c.-potentiostatic technique. A method similar to that suggested by Wolynec and Escalante [17] for determination of current density–potential curves of steel in stagnant NaCl solutions was adopted. Before imposition of each potential step, the system was left unpolarized for some minutes to allow the corroding system to return, at least partially, to the condition observed initially. At each value of polarization potential, current was determined by extrapolating the data of the current decay curves to infinite time.

Secondly, a simulated CP system was constructed consisting of a 25 cm diameter pipe and a platinized titanium 0.2 cm diameter wire anode. The pipe was placed vertically in a plastic container filled with the solution. The electrolyte level was kept 1 cm below the edge of the pipe in order to avoid end effects.

The anode was mounted between two plastic holders, one at the top and the other at the bottom of the pipe, which assured its vertical position. As well as at the central position, the measurements were conducted with the anode placed at each of six equally spaced locations on a radius connecting the center of the cathode with the point on the pipe positioned at 180° as shown in Figure 1.

Saturated calomel reference electrodes were placed at 0°, 90°, 180° and 270° (Figure 1) with Luggin capillary tips at approximately 3 mm from the pipe surface. While the electrical potential of the metal relative to the adjacent reference electrode at 0° was kept at a value of −700 mV, the potential at 180° was recorded as a function of time. During the initial stabilization and the relaxation of the system between two measurements, the electrical potential was also recorded at all four points at which the reference electrodes were placed.

4. Results and discussion

4.1. *Polarization measurements*

The electrochemical reactions occurring on the cathode are described by a current density–potential curve, which is nonlinear in nature and yields a boundary condition (c) of the form [18, 19]:

$$\boldsymbol{i} = \boldsymbol{i}_{\mathrm{a}} + \boldsymbol{i}_{\mathrm{l}} + \boldsymbol{i}_{\mathrm{c}} = \exp\left[\frac{2.303(E - E_{\mathrm{a}}^{*})}{b_{\mathrm{a}}}\right] - i_{\mathrm{l}} - \exp\left[\frac{-2.303(E - E_{\mathrm{c}}^{*})}{b_{\mathrm{c}}}\right] \qquad (11)$$

where

$$E_{\mathrm{a}}^{*} = E_{\mathrm{a}}^{\mathrm{e}} - \frac{b_{\mathrm{a}}}{2.303}\ln(i_{0\mathrm{a}}) \qquad (12a)$$

$$E_{\mathrm{c}}^{*} = E_{\mathrm{c}}^{\mathrm{e}} + \frac{b_{\mathrm{c}}}{2.303}\ln(i_{0\mathrm{c}}) \qquad (12b)$$

$E_{\mathrm{a}}^{\mathrm{e}}$ and $E_{\mathrm{c}}^{\mathrm{e}}$ are the equilibrium potentials for iron dissolution and hydrogen evolution, $i_{0\mathrm{a}}$ and $i_{0\mathrm{c}}$ are the corresponding exchange current densities and b_{a} and b_{c} are the anodic and the cathodic Tafel slopes.

The three terms on the right side of the Equation 11 are attributed to iron oxidation, oxygen reduction and hydrogen evolution, respectively (Figure 2). The amount of current apportioned to each reaction can be estimated by comparing the polarization data from runs in both the aerated and the deaerated solution.

A nonlinear current density–potential curve for iron and low-carbon steel in NaCl solutions of different concentrations and tap water was obtained from d.c.-potentiostatic measurements. Parameters i_{l}, E_{a}^{*}, E_{c}^{*}, b_{a} and b_{c} were determined by fitting the model Equation 11 to the experimental data. Tables 1 and 2 present the results of measurements in deaerated and aerated

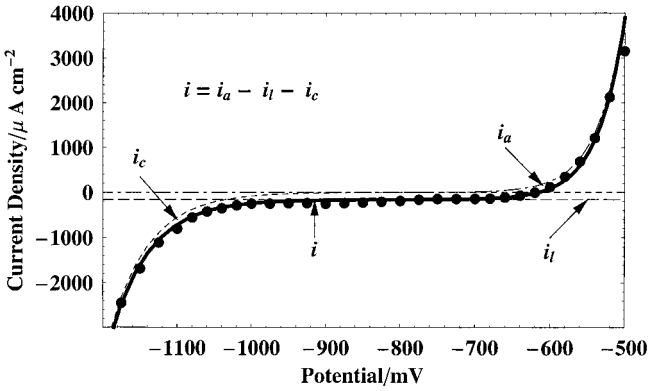

Fig. 2. A current density–potential curve for high-purity iron in 0.3% NaCl. (●) experimental points, (– · –) partial current density of iron dissolution i_{a}, (– –) partial current density of oxygen reduction i_{l}, (- - -) partial current density of hydrogen evolution i_{c}, (—) net current density i.

Table 1. Anodic corrosion parameters, current density at −700 mV vs SCE and corrosion velocity of high-purity iron and low-carbon steel in deaerated solutions

Metal	Solution /% by weight	b_{a} /mV dec^{-1}	E_{a}^{*} /mV vs SCE	i_{a} /μA cm^{-2} at −700 mV vs SCE	Corrosion velocity /mpy
High-purity iron	0.3% NaCl	60	−732	3.42	1.71
	tap water	60	−737	4.14	2.07
Low-carbon steel	1% NaCl	60	−720	2.15	1.08
	0.3% NaCl	59	−735	3.92	1.96
	tap water	58	−740	4.90	2.45

Table 2. Anodic corrosion parameters, current density at −700 mV vs SCE and corrosion velocity of high-purity iron and low-carbon steel in aerated solutions

Metal	Solution /% by weight	b_a /mV dec^{-1}	E_a^* /mV vs SCE	i_l /μA cm^{-2}	i_a /μA cm^{-2} at −700 mV vs SCE	Corrosion velocity /mpy
High-purity iron	0.3% NaCl	60	−732	65	3.42	1.71
	0.03% NaCl	59	−740	75	4.77	2.39
	tap water	61	−761	45*	10.01	5.00
Low-carbon steel	0.3% NaCl	60	−720	30	2.15	1.08
	0.03% NaCl	64	−667	35	0.30	0.15
	tap water	61	−740	18*	4.53	2.27

* Average oxygen concentration was 5 mg dm^{-3} in tap water and 9 mg dm^{-3} in NaCl solutions

solutions, respectively. The results confirm those reported previously [17, 19, 20] for similar systems under similar conditions (Table 3). The observed anodic Tafel slope of 60 mV dec^{-1} is often explained [21–23] in terms of the dissolution process occurring via an iron chloride complex as an intermediate absorbed under Temkin conditions.

The mean value of the cathodic Tafel slope b_c for the investigated solutions was found to be approximately 121 mV dec^{-1} and the value of the parameter E_c^* was around −788 mV.

To apply the model, it is essential to find the interval of protection potentials for which the boundary condition (4) holds approximately. The limits of this interval are not sharp, and generally differ from one system to another. The upper limit represents the polarization potential at which the corrosion ceases. Often this potential is near the reversible potential of a metal under operating conditions. In this particular case, the upper limit was taken to be −700 mV. The anodic partial current densities and the corresponding corrosion velocities at −700 mV (1 μA cm^{-2} ≈ 0.5 mpy) are shown in Tables 1 and 2.

The lower limit of the interval of protection potentials may be defined as the polarization potential for the onset of significant hydrogen evolution that could lead to the blistering of paint or the embrittlement of steel. For example, in the investigated systems, at −900 mV, the hydrogen evolution partial current density computed from Equation 11 amounts to approximately $i_l/4$.

4.2. *Measurements in simulated CP system*

Measurements in the simulated CP system were started by stabilization of the system during which the potential difference between the four reference electrodes and the metal was recorded as a function of time. The results of one such measurement in 0.3% NaCl are shown in Figure 3. The mean value of the measured corrosion potential was −620 mV. After a period of stabilization, potential difference of −700 mV was applied between the structure and reference electrode at 0°, (Figure 1) while the potential difference at 180° was recorded as a function of time (Figure 4).

Before polarizing for subsequent anode position, the system was left unpolarized until a potential close to the corrosion potential was recovered. Typical potential decay curves recorded at the four reference electrodes are shown in Figure 5.

Table 3. Anodic Tafel slopes of low-carbon steel in NaCl solutions from literature

Reference	Metal	Solution	b_a /mV dec^{-1}
[16]	Low-carbon steel	2.8 and 4% NaCl	59
[18]		0.001 M NaCl	64
[18]		0.01 M NaCl	68
[19]		Artificial sea water (Aquarium System, Ohio)	59

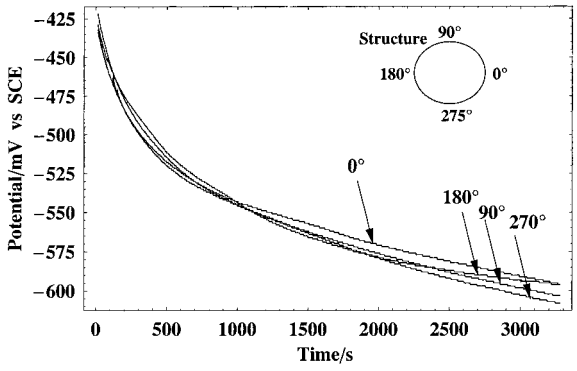

Fig. 3. Potential transients at four reference electrodes during stabilization of the simulated CP system in 0.3% NaCl.

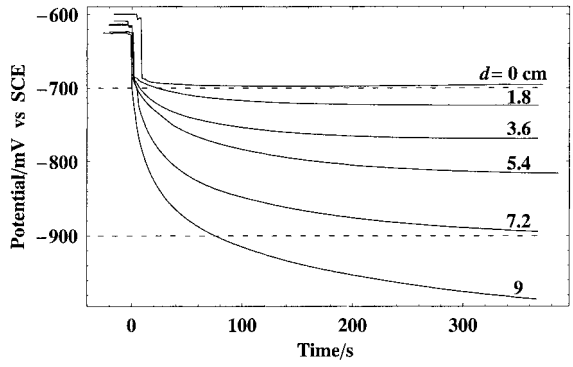

Fig. 4. Potential transients measured at the reference electrode positioned at 180° (Figure 1) during polarization of the pipe to −700 mV vs SCE, at 0°, in 0.3% NaCl.

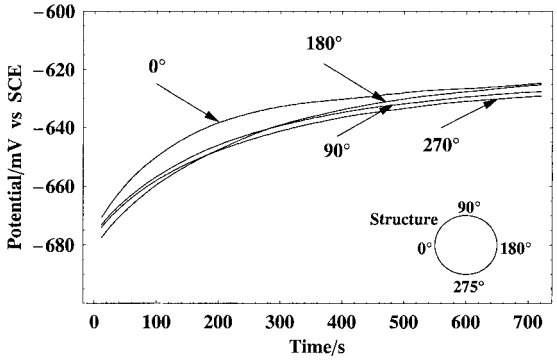

Fig. 5. Potential transients measured at four reference electrodes during relaxation of the simulated CP system in 0.3% NaCl.

Maximum variation of the local cathode potential $\Delta\Phi^{max}$ occurs between the point most distant from the anode (at 0°, Figure 1) and the point closest to the anode (at 180°, Figure 1). When a polarization potential of −700 mV is maintained at 0°, the potential at 180° may be considerably more negative and, accordingly, an appreciable portion of current may be used for the cathodic evolution of hydrogen.

The measurements in Figure 6 shows that $\Delta\Phi^{max} = 0$ when the anode is placed centrally (for $d = 0$), and increases by removing the anode from the centre of the cathode and by lowering the electrolyte conductivity. The full lines in Figure 6 represent the dependence predicted by the model.

After arbitrarily taking the value of the potential at all points adjacent to the anode as zero ($\Phi_a = 0$), the values of $\Delta\Phi^{max}$ may be reduced in the following way:

$$\Delta\Phi^{max}_{red} = \frac{\kappa}{i_l}\Delta\Phi^{max} \tag{13}$$

where

$$\Delta\Phi^{max} = \frac{\kappa}{i_l}\left[\Phi(u_c, 0) - \Phi(u_c, \pi)\right] \tag{14}$$

and $\Phi(u, v)$ is computed from the Equation 10.

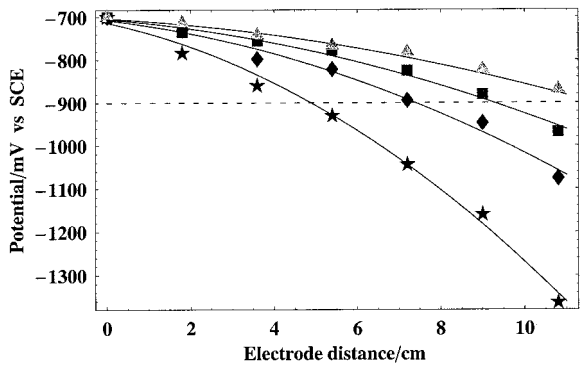

Fig. 6. Stationary-state potential measured at the reference electrode positioned at 180° (Figure 1) as a function of electrode distance d in electrolytes of different conductivities. Full lines represent dependency predicted by the model. Key: (▲) 1% NaCl, (■) 0.6% NaCl, (◆) 0.3% NaCl, (★) 0.15% NaCl.

Table 4. Output results of the model for various distances d of the anode-to-cathode centre

d /cm	u_a	u_c	a /cm	$\Delta\Phi^{max}_{red}$ /cm	n
1.8	6.75	1.94	42.50	7.25	4
3.6	5.99	1.24	19.90	14.82	7
5.4	5.46	0.84	11.77	23.12	10
7.2	4.98	0.55	7.24	32.81	15
9	4.43	0.33	4.18	45.37	24
10.8	−3.6	−0.15	−1.83	65.40	54

The model output is shown in Table 4 for various anode-to-cathode distances, d. n is the number of Fourier coefficients required for 0.1 mV computational precision.

Input parameters κ and i_l are shown in Table 5 along with the root mean square deviation of the computed from the measured data. Electrolyte conductivity κ is a measured quantity while i_l values were adjusted in order to achieve a good agreement between the measurements and the model. The adjusted values of i_l are in accord with those obtained from polarization measurements (Table 2).

After imposing the polarization potential, current transients were recorded. Average cathodic current densities in 0.3% NaCl are shown in Figure 7 as functions of time for varying anode-to-cathode distance d.

The increase in current passing through the system caused by the approach of the anode to the wall of the cathode is a direct consequence of nonlinearity of the current density–potential curve. It may be computed to a first approximation by entering the position-dependent

Table 5. Input parameters κ and i_l of the model and the root mean square deviation of the calculated against the measured data

Solution /% by weight	κ /mS cm^{-1}	i_l /μA cm^{-2}	RMS /mV
1% NaCl	14	39	24.0
0.6% NaCl	10	40	21.8
0.3% NaCl	5.5	31	24.4
0.15% NaCl	2.76	27.9	18.6

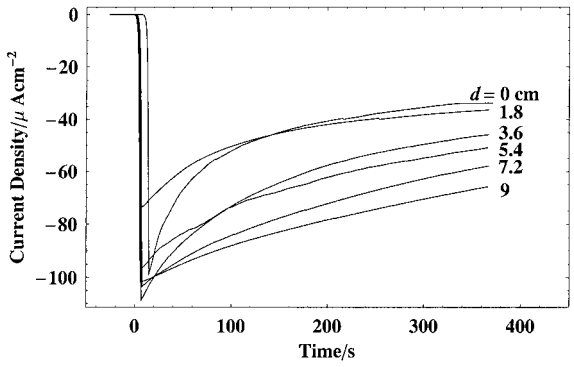

Fig. 7. Average cathode current density as a function of time for different anode-to-cathode distances in 0.3% NaCl.

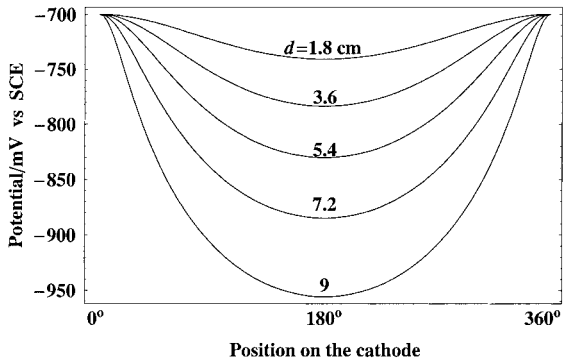

Fig. 8. Calculated potential distribution around the circumference of the pipe in 0.3% NaCl for different values of anode-to-cathode distances.

cathode polarization potentials obtained from Equation 9 into Equation 11 [2].

A computed distribution of the cathode polarization potential in 0.3% NaCl is shown in Figure 8. A corresponding distribution of current densities is shown in Figure 9. Average current densities on the cathode surface, computed for various anode positions, are shown in Table 6 (in 0.3% NaCl). By comparison of Figure 9 and the results in Table 6, it is observed that the experimental values are approximately 20 μA cm^{-2} higher than the computed ones, except for the, case of the anode positioned close to the cylinder axes. There are two probable reasons for this discrepancy: (i) steady state was not fully reached and, therefore, the measured currents are too large (endpoints of curves in Figure 7); (ii) in the first approximation, the computed increase of current is underestimated. However, a more realistic picture of the cathode current density distribution may be acquired by a numerical model in which nonlinearity of the cathode boundary condition could be taken into account and the computational procedure would become iterative.

The values of i_l from Table 5 that were entered as input parameters into the model were compared to the computed average current densities shown in Table 6. Values in the shaded cells (Table 6) differ significantly

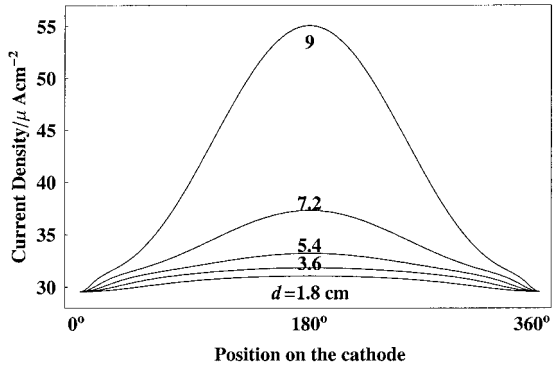

Fig. 9. Calculated distribution of current density around the circumference of the pipe in 0.3% NaCl for different values of anode-to-cathode distances.

Table 6. Average values of cathode current densities in μA cm^{-2} predicted by the model

d/cm	NaCl solution % by weight			
	1	0.6	0.3	0.15
1.8	38.11	39.27	30.46	27.76
3.6	38.54	39.76	31.05	28.99
5.4	38.91	40.24	31.82	33.78
7.2	39.34	40.97	33.76	64.44
9	40.10	42.91	41.75	–
10.8	42.37	53.62	121.79	–

from the initially assumed values. However, the model and the experimental data are in good agreement even in those particular cases, as seen from Figure 6. This may be attributed to the fact that the significant increase in local cathodic current density does not introduce significant changes in polarization potential due to the high slope of the cathodic current density–potential curve in this potential range.

5. Comparison of CP systems with one and two wire anodes

In the case of electrical potential fields, the principle of superposition holds. The mathematical analysis is extended to the case of two anodes by assuming that a half of the cathode current flows from each anode. Three-dimensional reduced potential distributions are shown in Figures 10 and 11 for one-anode and two-anode arrangements, respectively. Also shown in Figures 10 and 11 is the anode-to-cathode potential variation.

Comparison of $\Delta\Phi_{red}^{max}$ in Figures 10 and 11, shows that for the two-anode arrangement, maximum difference in the polarization potentials at the cylinder surface is reduced.

6. Conclusion

The applicability of a two-dimensional five-parameter model of the internal CP system of a cylindrical

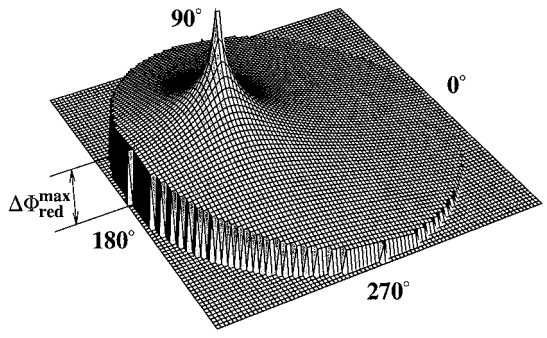

Fig. 10. Three-dimensional plot of the potential distribution in CP system with one wire anode placed at 5.4 cm from the cathode centre.

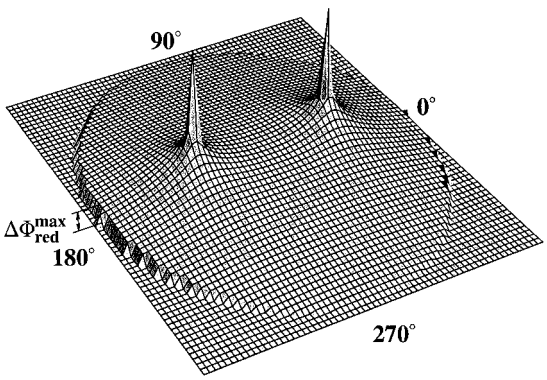

Fig. 11. Three-dimensional plot of the potential distribution in CP system with two wire anodes placed symmetrically at 5.4 cm from the cathode centre.

structure was investigated. When the geometric and electrochemical characteristics of the particular CP system that constitute the input parameters of the model can be measured or estimated with a certain degree of accuracy, provided that the conditions in the system resemble those presumed by the model, the model was shown to give a good estimation of the cathode potential distribution indicating the uniformity of the degree of protection achieved throughout the protected structure surface. The simplicity of the calculation makes the model particularly interesting for practical use.

References

1. G.A. Prentice and H Smyrl (Eds.), 'Perspectives in Corrosion', *AIChE Symposium Series no. 278*, vol. 86 (American Institute of Chemical Engineers, New York 1990), p. 22.
2. C. Wagner, *J. Electrochem. Soc.* **98** (1951) 116.
3. J.D. Jackson, 'Classical Electrodynamics', 2nd edn. (John Wiley & Sons, New York, 1975), p. 84.
4. F. Ayres and J. C. Ault, 'Differential Equations' (Schaum, New York, 1981), p. 82.
5. W.H. Press, B.P. Flannery, S.A. Teukolsky and W.T. Vetterling, 'Numerical Recipes in Pascal: The Art of Scientific Computing' (Cambridge University Press, Cambridge, 1990), p. 673.
6. B. Steffen and I. Rousar, *Electrochim. Acta* **40** (1995) 379.
7. C.A. Brebbia, J.C.F. Telles and L.C. Wrobel, 'Boundary Element Techniques' (Springer, Berlin, 1984), p. 47.
8. T.V. Hromadka and C. Lai, 'The Complex Variable Boundary Element Method in Engineering Analysis' (Springer, New York, 1987), p. 20.
9. C. Wagner, *J. Electrochem. Soc.* **99** (1952) 1.
10. C. Wagner, *J. Electrochem. Soc.* **104** (1957) 631.
11. J. Newman, *J. Electrochem. Soc.* **138** (1991) 3354.
12. J. Newman, *J. Electrochem. Soc.* **144** (1997) 450.
13. R.V. Churchill and J.W. Brown, 'Fourier Series and Boundary Value Problems' (McGraw Hill, New York, 1987), p. 17.
14. P. Moon and D.E. Spencer, 'Field Theory Handbook' (Springer-Verlag, Berlin, 1961), p. 89.
15. M.P. Morse and H. Feshbach, 'Methods of Theoretical Physics' (McGraw Hill, New York, 1953), p. 1210.
16. R.S. Murray, 'Vector Analysis' (Schaum, New York, 1959), p. 140.
17. S. Wolynec and E. Escalante, *Corrosion* **36** (1980) 327.
18. J.O'M. Bockris and A.K.N. Reddy, 'Modern Electrochemistry', vol. 2 (Plenum Press, New York, 1977), p. 1267.
19. J.F. Yan, S.N.R. Pakalapati, T.V. Nguyen and R.E. White, *J. Electrochem. Soc.* **139** (1992) 1932.
20. T.P. Hoar and T.W. Farer, *Corrosion Sci.* **1** (1961) 49.
21. M. Duprat (Ed.), 'Electrochemical Methods in Corrosion Research', vol. 8 (Trans. Tech. Publications, Switzerland, 1986), p. 429.
22. S. Asakura and K. Nobe, *J. Electrochem. Soc.* **118** (1971) 19.
23. W.J. Lorenz, *Corrosion Sci.* **5** (1965) 121.